Solar flare impacts on ionospheric electrodyamics

Liying Qian,[1] Alan G. Burns,[1] Stanley C. Solomon,[1] and Phillip C. Chamberlin[2]

Received 27 January 2012; revised 22 February 2012; accepted 23 February 2012; published 20 March 2012.

[1] The sudden increase of X-ray and extreme ultra-violet irradiance during flares increases the density of the ionosphere through enhanced photoionization. In this paper, we use model simulations to investigate possible additional contributions from electrodynamics, finding that the vertical E × B drift in the magnetic equatorial region plays a significant role in the ionosphere response to solar flares. During the initial stage of flares, upward E × B drifts weaken in the magnetic equatorial region, causing a weakened equatorial fountain effect, which in turn causes lowering of the peak height of the F_2 region and depletion of the peak electron density of the F_2 region. In this initial stage, total electron content (TEC) enhancement is predominantly determined by solar zenith angle control of photoionization. As flares decay, upward E × B drifts are enhanced in the magnetic equatorial region, causing increases of the peak height and density of the F_2 region. This process lasts for several hours, causing a prolonged F_2-region disturbance and TEC enhancement in the magnetic equator region in the aftermath of flares. During this stage, the global morphology of the TEC enhancement becomes predominantly determined by these perturbations to the electrodynamics of the ionosphere. **Citation:** Qian, L., A. G. Burns, S. C. Solomon, and P. C. Chamberlin (2012), Solar flare impacts on ionospheric electrodyamics, *Geophys. Res. Lett.*, *39*, L06101, doi:10.1029/2012GL051102.

1. Introduction

[2] Solar flares produce large and rapid increases of solar X-ray and extreme-ultraviolet (EUV) radiation. These rapid increases directly enhance ionization in the upper atmosphere, causing "sudden ionospheric disturbances" (SID), which disrupts navigation systems and communications that rely on ionosphere electron density. Consequently, many phenomena associated with SID, including short wave fadeout, sudden phase anomalies, and (magnetic) solar flare effects, have been investigated since the 1950s [e.g., *Shain and Mitra*, 1954; *Mendillo et al.*, 1974; *Davies*, 1990; *Manju and Viswanathan*, 2005]. Most ionosphere responses to solar flares have been attributed to, and can be explained by, the enhancement of solar X-rays and EUV during solar flares. For example, it has been found that total electron content (TEC) enhancement during solar flares primarily follows the cosine of solar zenith angle [*Zhang and Xiao*, 2003; *Liu et al.*, 2007; *Qian et al.*, 2011]. However, recent measurements have revealed phenomena that may not be attributable to or cannot be explained by solar irradiance and related physical and chemical processes. Using high temporal cadence observations of TEC by the ground–based GPS network, *Tsurutani et al.* [2005] found that the TEC disturbance during an X17 flare that occurred on October 28, 2003 lasted for several hours, much longer than the flare duration. They considered that the long TEC disturbance is due to the slow recombination rate at higher altitudes. Recent measurements of electron density at high temporal and spatial resolution by the Challenging Minisatellite Payload (CHAMP) satellite revealed the weakening of equatorial ionization anomaly (EIA) and enhancement of electron density at the magnetic equator during the X17 flare that occurred on October 28, 2003 [*Liu et al.*, 2007], suggesting electrodynamical changes during solar flares. These observations raise the questions that are the basis for this study: Do electrodynamical effects play a significant role in the ionosphere response to solar flares, and how do electrodynamics affect the time evolution of ionosphere parameters, including TEC, and the peak density (N_mF_2) and height (h_mF_2) of the F_2-region electron density profile?

2. Model Description

2.1. NCAR TIME-GCM

[3] Here, we use a first principles upper atmosphere general circulation model with full flare spectra to investigate whether and how electrodynamics affect flare responses in the ionosphere. The first principles model is the National Center for Atmospheric Research (NCAR) Thermosphere-Ionosphere-Mesosphere-Electrodynamics General Circulation Model (TIME-GCM) [*Roble and Ridley*, 1994]. The NCAR TIME-GCM solves the fully coupled, nonlinear, hydrodynamic, thermodynamic, and continuity equations of the neutral gas, and the ion and electron energy and momentum equations, and the ion continuity equation self-consistently. It utilizes a spherical coordinate system fixed with respect to the rotating Earth, with latitude and longitude as the horizontal coordinates and pressure surface as the vertical coordinate. It has a horizontal resolution of 5° × 5°. The pressure interfaces are defined as $lev = \ln(P_0/P)$, where P_0 is a reference pressure at $5 \times 10^{-4}\mu$b. The model has 49 pressure surfaces covering the altitude range from ~30 km to ~700 km, with *lev* ranging from −17 to 7 and a vertical resolution of one half scale height. For the investigation in this paper, we will use solar spectra provided by the Flare Irradiance Spectral Model (FISM) [*Chamberlin et al.*, 2007, 2008] as the solar input for the TIME-GCM.

2.2. FISM Solar Flare Model

[4] High temporal (1 minute) flare spectra (0–190 nm with 1 nm resolution) calculated by FISM [*Chamberlin et al.*, 2007, 2008] were used as solar input to the TIME-GCM. FISM is an empirical model developed for space weather

[1]High Altitude Observatory, National Center for Atmospheric Research, Boulder, Colorado, USA.
[2]Solar Physics Laboratory, NASA Goddard Space Flight Center, Greenbelt, Maryland, USA.

0094-8276/12/2012GL051102

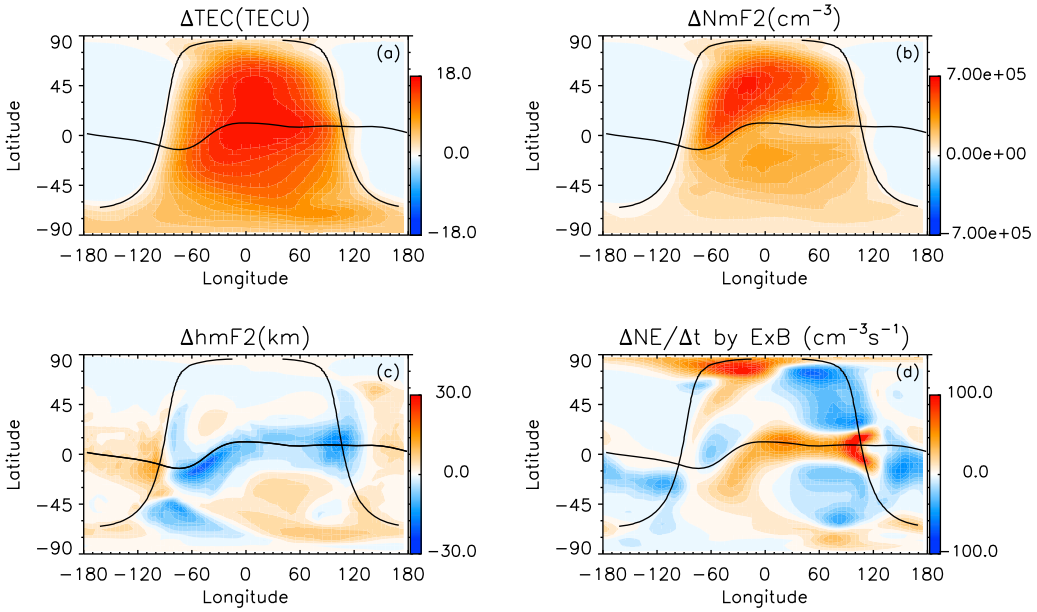

Figure 1. Horizontal maps of the ionosphere responses to the X17 flare that occurred on October 28, 2003 (peak soft X-ray response at 11:10UT) at 11:30UT. (a) Change of TEC; (b) change of N_mF_2; (c) change of h_mF_2; and (d) rate of change of electron density due to vertical E × B drifts at *lev* = 2 (*lev* = ln(P_0/P), P_0 = 5 × 10^{-4} μb). Also plotted in the figure are the terminator and magnetic equator.

applications. It uses the GOES XRS 0.1–0.8 nm channel, TIMED SEE, SORCE (Solar Radiation and Climate Experiment) SOLSTICE (SOLar STellar Irradiance Comparison Experiment) [*McClintock et al.*, 2000], and F10.7 as inputs, to estimate the solar X-ray and EUV irradiances at wavelengths from 0 to 190 nm at 1 nm resolution with a temporal resolution of 60 seconds [*Chamberlin et al.*, 2007, 2008]. This is a high enough temporal resolution to model variations due to solar flares, for which few accurate measurements at these wavelengths exist.

3. Results

[5] We conducted investigations to an X17 flare that occurred on 2003301 (10/28/2003). Based the soft X-ray (0.1–0.8 nm) observed by the Geostationary Operational Environmental Satellites (GOES), the X17 flare started at ∼11:00UT, peaked at ∼11:10UT, and decayed about 1 hour later at ∼12:00UT. Geomagnetic activity on October 28, 2003 as well as on October 27, 2003 was between low to moderate (Kp ∼ 3). Observational studies of this flare have been conducted for both the thermosphere [e.g., *Sutton et al.*, 2006; *Liu et al.*, 2007] and the ionosphere [e.g., *Tsurutani et al.*, 2005; *Liu et al.*, 2007]. Modeling studies of this flare have also been conducted for the thermosphere [e.g., *Pawlowski and Ridley*, 2008; *Qian and Solomon*, 2011]. Here we focus on modeling studies of ionosphere responses to this flare. The TIME-GCM was run using FISM daily spectra starting 25 days prior to the date of the X17 flare. The model output at the beginning of October 28, 2003 was then used as initial conditions to conduct two model runs. In the first run the model used FISM flare spectra for October 28, 2003, whereas it used FISM daily spectrum (excluding flares) for October 28, 2003 in the second run. The difference fields from these two model runs (the first run minus the second run) were used to analyze flare effects in the ionosphere as well as physical processes and mechanisms for the flare effects.

[6] The simulation results show that, as we already know [e.g., *Zhang et al.*, 2003; *Xiong et al.*, 2011], the ionosphere responded immediately to the enhancement of the solar X-ray and EUV, with increased electron density throughout the ionosphere and a TEC enhancement following the solar zenith angle control of photoionization. However, we also see that other ionosphere parameters responded instantly to the flare, particularly in the magnetic equator region. Figure 1 shows the changes between the first model run (flare run) and the second model run (no flare run) for TEC (Figure 1a), N_mF_2 (Figure 1b), and h_mF_2 (Figure 1c), as well as the rate of change of electron density ($\partial Ne/\partial t$) due to vertical E × B drift ($-\partial(wi \times Ne)/\partial z$, where wi is the vertical ion velocity due to the E × B force) (Figure 1d) at 11:30UT, 20 minutes after the peak X-ray of the X17 flare at 11:10UT. The rate of change of electron density due to the vertical E × B drift is at pressure level 2 of the model. At the magnetic equator, this was about 400 km, just below the $F2$ peak. There are distinct features along the magnetic equator. h_mF_2 decreased (Figure 1c), the rate of change of electron density due to the vertical E × B drift was positive below the $F2$ peak along the magnetic equator (Figure 1d), which increases the electron density in this region. The lowering of h_mF_2 caused depletion of N_mF_2 (Figure 1b). Diagnostic analysis shows that these changes of the ionosphere parameters were caused by the weakening of the upward E × B drift along the magnetic equator in response to the solar flare. The weakened upward E × B drift caused weakening of the equatorial fountain effect. This is consistent with CHAMP observations that the EIA crests moved closer to the magnetic equator immediately following the X17 flare that occurred on October 28, 2003 [*Liu et al.*, 2007], indicating weakening of upward E × B drifts along the magnetic equator. The resulting enhancement of electron

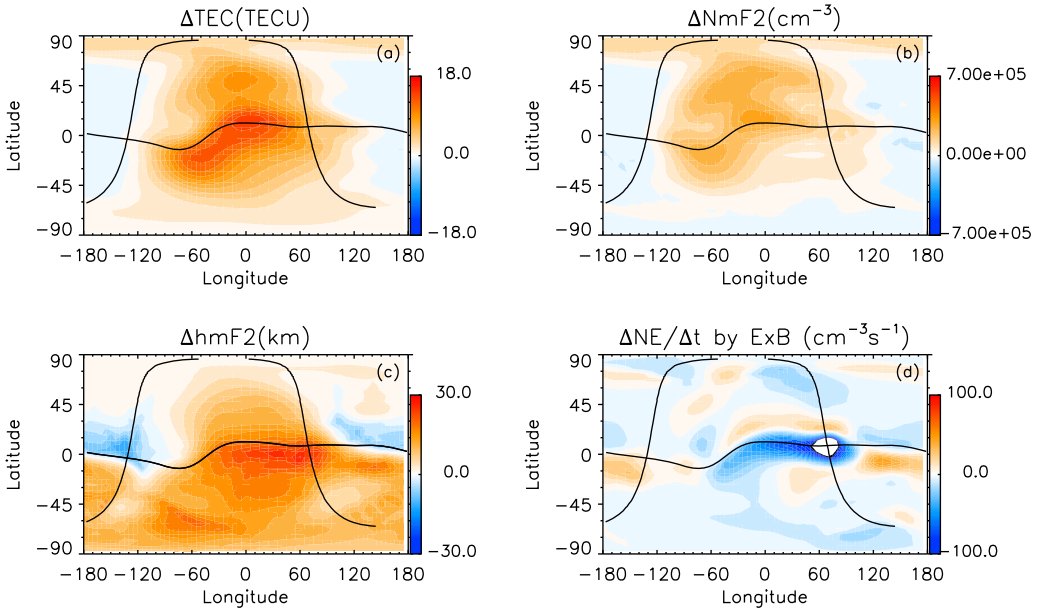

Figure 2. Horizontal maps of the ionosphere responses to the X17 flare that occurred on October 28, 2003 (peak soft X-ray response at 11:10UT) at 14:00UT. (a) Change of TEC; (b) change of N_mF_2; (c) change of h_mF_2; and (d) rate of change of electron density due to vertical E × B drifts at *lev* = 2 (*lev* = ln(P_0/P), $P_0 = 5 \times 10^{-4}\mu$b). Also plotted in the figure are the terminator and magnetic equator.

density at 400 km (Figure 1d), just below the *F*2 peak, during this initial response stage, was also observed by CHAMP [*Liu et al.*, 2007]. Our diagnostic analysis shows that the weakening of the upward E × B drift caused the *F*2 peak to drop to lower pressure surfaces in the magnetic equatorial region. During this initial stage, TEC enhancement is predominantly determined by solar zenith angle control of photoionization (Figure 1a). The weakening of the upward E × B drift in the magnetic equatorial region lasted for about 1 hour after the GOES X-ray peak at 11:10UT, and ended when the flare decayed at around 12:00UT.

[7] The weakening of the upward E × B drift in the magnetic equatorial region is caused by weakening of the eastward E field. The weakening of the eastward electric field can be caused by changes of the conductivity distribution resulting from changes of electron density during solar flares. Large enhancement of electron density in the *E* region increases both Hall and Pedersen conductivities, and increases the field-line integrated Hall-to-Pedersen conductivity ratio in the equatorial to low latitude region, which can in turn cause weakened eastward electric field [*Richmond*, 1973].

[8] The ionosphere responses shown in Figure 1 evolved with time, reaching the state given in Figure 2 at 14:00UT, about 3 hours following the X-ray peak. The TEC enhancement along the magnetic equator became the dominant feature compared to the solar zenith angle effect (Figure 2a). Both h_mF_2 and N_mF_2 increased (Figures 2b and 2c) in the region. The rate of change of electron density due to the vertical E × B drift was negative just below the *F*2 peak in the magnetic equatorial region (Figure 2d), which had the effect of decreasing electron density in the region. Diagnostic analysis shows that after the weakening of the upward E × B drift ended around 12:00UT when the flare decayed, the upward E × B drift enhanced along the magnetic equator, which caused enhanced equatorial fountain effect and drove the changes of ionosphere parameters shown in Figure 2. The magnitude of the enhancement of the upward E × B drift was about 30% of the magnitude of the initial weakening of the upward E × B drift. However, the enhancement of the upward E × B drift lasted for more than 3 hours, much longer than the initial weakening of the upward E × B drift. This extended enhancement of the upward E × B drift is caused by enhancement of eastward electric field. As the flare decays, the *E* region recovers faster than the *F* region. Consequently, the field-line integrated Hall-to-Pedersen conductivity ratio can decrease, which corresponds to enhanced eastward electric field [*Richmond*, 1973]. In addition, enhanced *F*-region dynamo resulting from disturbed neutral wind in response to the flare can also contribute to the enhancement of the eastward electric field.

[9] Figure 3 shows the change of vertical ion velocity (Figure 3a), the rate of change of electron density due to the vertical E × B drift (Figure 3b), and the change of electron density (Figure 3c) at12:00 local time at the magnetic equator , in response to the X17 flare. Vertical ion velocity does not change much with altitude. Plotted in Figure 3a is the change of vertical ion velocity in response to the flare at *lev* = 2, which is about 400 km (Figures 3b and 3c). The vertical ion velocity responded immediately to the flare (weakening of the upward E × B drift), reached maximum decrease of ∼3 m/s shortly after the peak soft X-ray enhancement at 11:10UT. Then the velocity started to recover and returned to the pre-flare velocity at ∼12:00UT, closely following the course of the soft X-ray changes during the flare. After ∼12:00UT, the velocity increased, reached a maximum enhancement of ∼1 m/s at ∼13:30UT, then started to recover. The maximum enhancement in this later stage is about 30% of the maximum decrease in the initial stage, but lasted much longer (ended at ∼16:00UT).

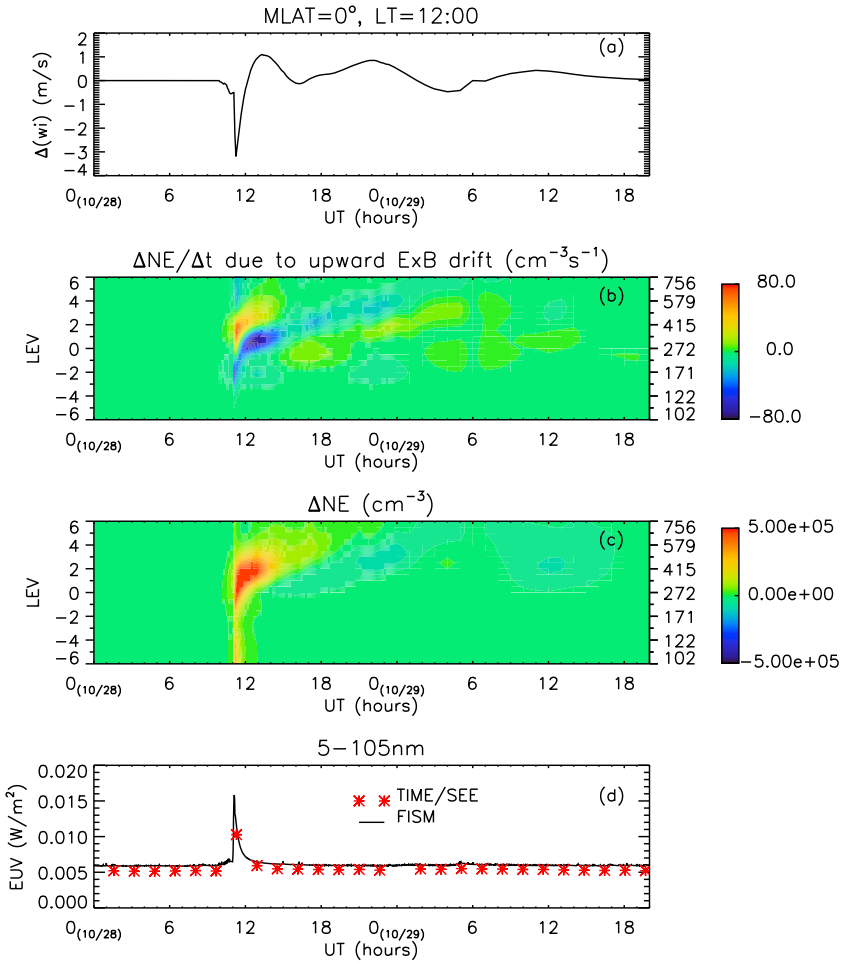

Figure 3. Time series of ionosphere responses to the X17 flare that occurred on October 28, 2003. (a) Change of vertical plasma velocity (vertical E × B drifts) at *lev* = 2 (*lev* = ln(P_0/P), $P_0 = 5 \times 10^{-4}$ μb), at 12:00LT at the magnetic equator; (b) rate of change of electron density due to the vertical E × B drifts at 12:00LT at the magnetic equator; (c) change of electron density at 12:00LT at the magnetic equator; (d) integrated EUV from 5–105 nm calculated by FISM (black line) and observed by TIMED SEE (red star).

Effects of the initial weakening of the upward E × B drift and the extended enhancement of the upward E × B drift later on are shown in Figures 3b and 3c. During the initial stage, the rate of change of electron density by the vertical E × B drift was negative above the *F*2 peak (reduction of electron density) but positive below the *F*2 peak (enhancement of electron density) (Figure 3b). When the E × B drift started to enhance at ∼12:00UT, the rate of change of electron density by the E × B drift was positive above the *F*2 peak (enhancement of electron density), but negative below the *F*2 peak (reduction of electron density (Figure 3b). Electron density in the *E* and *F*1 regions responded to the flare immediately but recovered to the pre-flare condition approximately 1 hour later at around 12:00UT. However, electron density enhancement near and above the *F*2 peak lasted for more than 4 hours after the flare peak, much longer than the responses in the *E* and *F*1 regions (Figure 3c). After 16:00UT, the upward E × B drift continued to fluctuate with smaller amplitudes, and finally returned to its pre-flare condition about 24 hours later (at ∼17UT on October 29, 2003) (Figure 3a). These small fluctuations caused minor changes of electron density (Figure 3c). The ionosphere completely returned to its pre-flare conditions at ∼17:00UT on October 29, 2003. The e-folding time of the TEC decay in the magnetic equator region is ∼4–6 hours. This is much longer than the flare irradiance decay rate. Figure 3d shows the integrated EUV (5–105 nm) calculated by FISM and observed by TIMED SEE (∼14 orbits per day). The e-folding time of the EUV decay is 20 minutes for this flare. It is important to note that time series of the flare responses can be viewed either at a fixed local time or at a fixed longitude. Time series at a fixed local time would incur a longitudinal variation whereas time series at a fixed longitude would incur a local time variation. Therefore, we looked at times series at a fixed longitude (0°E) as well, and we obtained similar results and reached the same conclusions that we drew from Figure 3.

[10] In Figure 4, we compare TEC maps at 11:00UT (pre-flare) (Figures 4a and 4b), 11:30UT (the universal time of Figure 1) (Figures 4c and 4d), and 14:00UT (the universal time of Figure 2) (Figures 4e and 4f) observed by the ground based GPS TEC network and simulated by the TIME-GCM. Although the TEC maps observed by the GPS have limited spatial coverage, they still give evidence that the TIME-GCM simulated TEC maps are fairly reasonable compared

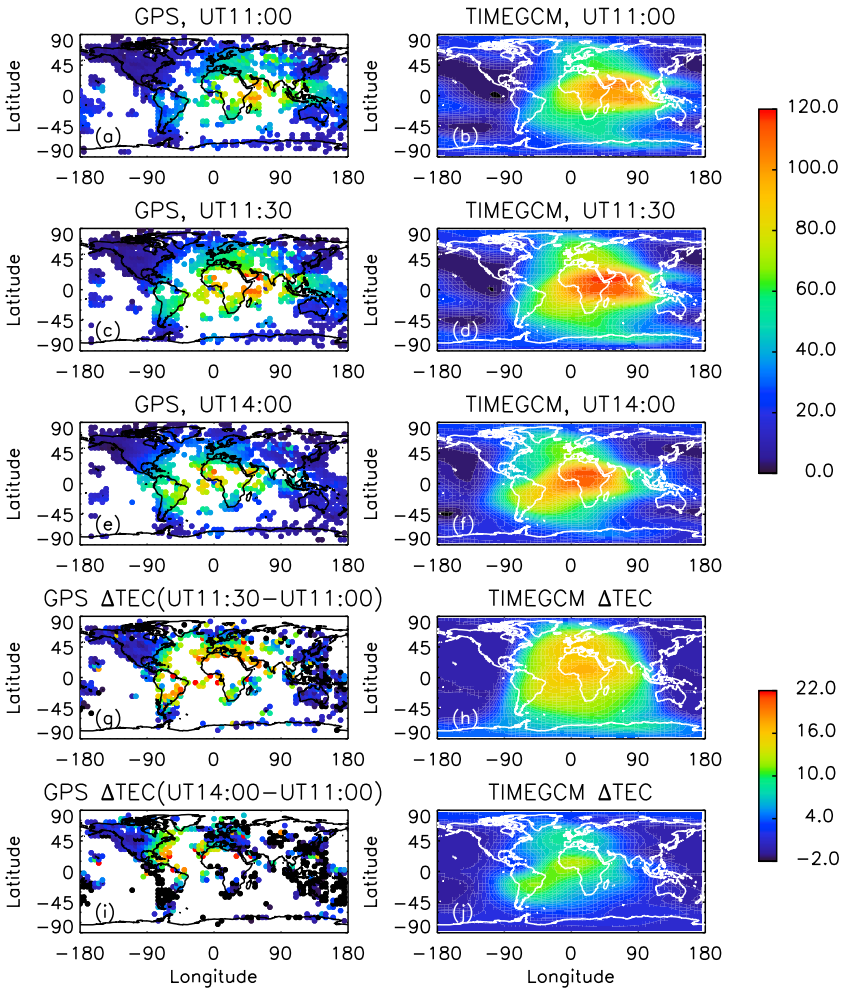

Figure 4. Global TEC observed by the ground based GPS TEC network and simulated by the TIME-GCM. (a) GPS TEC at 11:00UT (pre-flare); (b) TIME-GCM TEC at 11:00UT (pre-flare); (c) GPS TEC at 11:30UT (20 minutes after the X-ray peak); (d) TIME-GCM TEC at 11:30UT (20 minutes after the X-ray peak); (e) GPS TEC at 14:00UT (∼3 hours after the X-ray peak); (f) TIME-GCM TEC at 14:00UT (∼3 hours after the X-ray peak); (g) TEC difference between 11:30UT and 11:00UT observed by GPS; (h) TEC enhancement at 11:30UT simulated by TIME-GCM; (i) TEC difference between 14:00UT and 11:00UT observed by GPS; (j) TEC enhancement at 14:00UT simulated by TIME-GCM.

to the data. Figure 4g shows the GPS TEC difference between 11:00UT and 11:30UT. The TEC difference was calculated by subtracting the TEC difference between 11:00UT and 11:30UT on October 27, 2011 from the TEC difference between 11:00UT and 11:30UT on October 28, 2011. Figure 4i is the same as Figure 4g except that it shows the TEC difference between 11:00UT and 14:00UT. The purpose of subtracting the TEC difference on the previous day is to account for local time effects [*Tsurutani et al.*, 2005; *Qian et al.*, 2010, 2011]. Figures 4h and 4j are the TEC enhancements at 11:30UT and 14:00UT, respectively, simulated by the TIME-GCM. The TEC enhancement at 14:00UT, nearly 3 hours after the X-ray peak of the X17 flare, are evident from both the data (Figure 4i) and the model results (Figure 4j), although these enhancements are weaker than those at 11:30UT (Figures 4g and 4h).

4. Summary and Conclusions

[11] In this paper, we investigated solar flare impacts on ionosphere electrodynamics. We found that the main electrodynamical effects occurred in the magnetic equatorial region. During the initial stage of the flare, upward E × B drifts in the magnetic equatorial region weakened, which reduced the equatorial fountain effect. Consequently, the peak height of the F_2-region decreased, which in turn caused the depletion of the peak electron density of the F_2-region. Electron density decreased above the $F2$ peak but increased below the $F2$ peak. During this stage, TEC enhancement is predominantly determined by solar zenith angle effects of photoionization.

[12] The weakening of the E × B drift ended as the flare decayed. The upward E × B drift enhanced afterwards along the magnetic equator, which caused enhanced equatorial fountain effect. In the magnetic equatorial region, the enhanced E × B drift increased h_mF_2 and N_mF_2, increased TEC, and increased electron density above the $F2$ peak but decreased electron density below the $F2$ peak. The magnitude of the maximum enhancement of the upward E × B drift was weaker (∼30%) than the maximum magnitude of the initial weakening of the upward E × B drift, but the enhancement of the upward E × B drift lasted much longer.

This prolonged enhancement of the upward E × B drift caused prolonged F_2-region disturbance. The morphology of TEC enhancement changed from solar zenith angle driven to an E × B drift-driven phenomenon along the magnetic equator. The e-folding time of the TEC decay in the magnetic equator region is ∼4–6 hours, much longer than the EUV decay rate, which is 20 minutes for this flare.

[13] The reduced EIA crest separation observed by CHAMP [*Liu et al.*, 2007] confirms the predicted weakening of E × B drift and the resulting decreases of h_mF_2 and depletion of N_mF_2 in the magnetic equatorial region during the initial stage of flare responses. However, more observations of flare responses of ionosphere parameters in the magnetic equatorial region, including TEC, electron density profiles, and h_mF_2 and N_mF_2, should be conducted to confirm the E × B effects predicted by the model simulations, particularly during the prolonged later stage. In addition, future work is to investigate mechanisms of the weakening of the E × B drift in the magnetic equatorial region during the initial response to solar flares and the enhancement of the E × B drift during the prolonged later stage.

[14] **Acknowledgments.** This research was supported by NASA grants NNX08AQ31G and NNX09AJ60G to the National Center for Atmospheric Research. We would also like to acknowledge the Center for Integrated Space Weather Modeling (CISM) which is funded by the National Science Foundation's STC program under agreement ATM-0120950. NCAR is sponsored by the National Science Foundation.

[15] The Editor thanks Thomas Woods and an anonymous reviewer for their assistance in evaluating this paper.

References

Chamberlin, P. C., T. N. Woods, and F. G. Eparvier (2007), Flare Irradiance Spectral Model (FISM): Daily component algorithms and results, *Space Weather*, *5*, S07005, doi:10.1029/2007SW000316.

Chamberlin, P. C., T. N. Woods, and F. G. Eparvier (2008), Flare Irradiance Spectral Model (FISM): Flare component algorithms and results, *Space Weather*, *6*, S05001, doi:10.1029/2007SW000372.

Davies, K. (1990), *Ionospheric Radio*, Peter Peregrinus, London, doi:10.1049/PBEW031E.

Liu, H., H. Lühr, S. Watanabe, W. Köhler, and C. Manoj (2007), Contrasting behavior of the thermosphere and ionosphere in response to the 28 October 2003 solar flare, *J. Geophys. Res.*, *112*, A07305, doi:10.1029/2007JA012313.

Manju, G., and K. S. Viswanathan (2005), Response of the equatorial electrojet to solar flare related X-ray flux enhancement, *Earth Planets Space*, *57*, 231–242.

McClintock, W. E., G. J. Rottman, and T. N. Woods (2000), Solar STellar Irradiance Comparison Experiment II (SOLSTICE II) for the NASA Earth Observing System's Solar Radiation and Climate Experiment (SORCE) mission, *Proc. SPIE*, *4135*, 225–234, doi:10.1117/12.494220.

Mendillo, M., et al. (1974), Behavior of the ionospheric F region during the great solar flare of August 7, 1972, *J. Geophys. Res.*, *79*(4), 665–672, doi:10.1029/JA079i004p00665.

Pawlowski, D. J., and A. J. Ridley (2008), Modeling the thermospheric response to solar flares, *J. Geophys. Res.*, *113*, A10309, doi:10.1029/2008JA013182.

Qian, L., and S. C. Solomon (2011), Thermospheric density: An overview of temporal and spatial variations, *Space Sci. Rev.*, doi:10.1007/s11214-011-9810-z, in press.

Qian, L., A. G. Burns, P. C. Chamberlin, and S. C. Solomon (2010), Flare location on the solar disk: Modeling the thermosphere and ionosphere response, *J. Geophys. Res.*, *115*, A09311, doi:10.1029/2009JA015225.

Qian, L., A. G. Burns, P. C. Chamberlin, and S. C. Solomon (2011), Variability of thermosphere and ionosphere responses to solar flares, *J. Geophys. Res.*, *116*, A10309, doi:10.1029/2011JA016777.

Richmond, A. D. (1973), Equatorial electrojet. I. Development of a model including winds and instabilities, *J. Atmos. Terr. Phys.*, *35*, 1083–1103, doi:10.1016/0021-9169(73)90007-X.

Roble, R. G., and E. C. Ridley (1994), A thermosphere-ionosphere-mesosphere-electrodynamics general circulation model (TIME-GCM): Equinox solar cycle minimum simulations (30–500 km), *Geophys. Res. Lett.*, *21*, 417–420, doi:10.1029/93GL03391.

Shain, C. A., and A. P. Mitra (1954), Effects of solar flares on the absorption of 18.3 Mc/s cosmic noise, *J. Atmos. Terr. Phys.*, *5*, 316–328, doi:10.1016/0021-9169(54)90050-1.

Sutton, E. K., J. M. Forbes, R. S. Nerem, and T. N. Woods (2006), Neutral density response to the solar flares of October and November, 2003, *Geophys. Res. Lett.*, *33*, L22101, doi:10.1029/2006GL027737.

Tsurutani, B. T., et al. (2005), The October 28, 2003 extreme EUV solar flare and resultant extreme ionospheric effects: Comparison to other Halloween events and the Bastille Day event, *Geophys. Res. Lett.*, *32*, L03S09, doi:10.1029/2004GL021475.

Xiong, B., et al. (2011), Ionospheric response to the X-class solar flare on 7 September 2005, *J. Geophys. Res.*, *116*, A11317, doi:10.1029/2011JA016961.

Zhang, D. H., and Z. Xiao (2003), Study of ionospheric total electron content response to the great flare on 15 April 2001 using International GPS Service network for the whole sunlit hemisphere, *J. Geophys. Res.*, *108*(A8), 1330, doi:10.1029/2002JA009822.

A. G. Burns, L. Qian, and S. C. Solomon, High Altitude Observatory, National Center for Atmospheric Research, 3080 Center Green Dr., Boulder, CO 80301, USA. (lqian@ucar.edu)

P. C. Chamberlin, Solar Physics Laboratory, NASA Goddard Space Flight Center, Code 671, Greenbelt, MD 20771, USA.